Shape Recognition and Growth Measurement of Micropropagated Sugarcane Shoots

Yutaka Kaizu, Tsuguo Okamoto, Kenji Imou

Department of Biological and Environmental Engineering
Graduate School of Agricultural and Life Sciences
The University of Tokyo
Yayoi 1-1-1, Bunkyo-ku, Tokyo 113-8657, Japan
akaizu@mail.ecc.u-tokyo.ac.jp

Abstract

Machine vision algorithms were developed for shape recognition of ex vitro micropropagated sugarcane shoots. Shape features, such as stem axis angle, position and degree of growth required for robotic sorting and transplanting systems, were measured by a newly developed program. The stem axis angle was measured using the Hough transformation. The degree of growth was defined as the distance between the lower end of the stem and the +1 leaf's dewlap. The lower end of the stem was located by width adaptive template matching. The +1 leaf's dewlap was identified based on the curvature of its boundary. The algorithms are applicable for shape recognition of the sugarcane shoots in this stage.
[Keywords] micropropagation, sugarcane shoot, robotics, image processing, shape recognition, dewlap, curvature

Introduction

Sugarcane is the only agronomic crop that has been commercially micropropagated. Sugarcane originally propagates vegetatively whereas most agronomic crops such as rice, wheat and barley propagate by seed (Redenbaugh, 1990). Thus it is easy to adopt the micropropagation method to sugarcane.

Conventionally, sugarcane is grown from pieces of mature sugarcane cut into 40-centimeter lengths. Each seed cane has two buds, from which shoots emerge (Miyazato, 1986). Since sugarcane multiplies ten times a year, about 10% of farmland is used for producing the seed cane (Taba et al., 1998). Sugarcane is produced only in the southern islands of Japan, for historical and geographical reasons. Although Japan produces only 0.13% of the total world sugarcane product (FAOSTAT, 2002), its production has been indispensable to the regional economy of these small islands, both in terms of agriculture and the sugar manufacturing industry.

The harvested area of sugarcane has been decreasing for the last ten years in Kagoshima prefecture, because of the aging of farmers, abandonment of farming, young farmers changing to more profitable crops, and the lack of fully mechanized farming. As a countermeasure, Nansei Togyo Co., Ltd. in Tokunoshima Island has been producing and popularizing micropropagated sugarcane.

The advantages of micropropagated sugarcane are as follows.

1 Micropropagated sugarcane generates more seed cane, so the area set aside for producing it can be reduced and the area for harvesting sugarcane can be increased (Taba et al., 1998).
2 Micropropagated sugarcane propagates more rapidly, so a new cultivar can spread quickly.
3 The yield per unit area is higher (Teruya and Tokumoto, 1999).

Kaizu, Y., T. Okamoto, and K. Imou. "Shape recognition and Growth Measurement of Micropropagated Sugarcane". Agricultural Engineering International: the CIGR Journal of Scientific Research and Development. Manuscript IT 02 003. Vol. IV. October 2002.

In Tokunoshima Island, Nansei Togyo has been selling micropropagated sugarcane shoot since 2000, and sales have been growing steadily. The present price is 65 yen ($0.50) per shoot. However, the shoot supplier makes no profit at this price, so the production cost must be reduced in order to make the production of the shoots a new business in the region and to promote the use of micropropagated sugarcane shoot on other islands. To reduce the production costs, the company has been mechanizing micropropagation in cooperation with the authors.

There are five growing stages in micropropagation (Debergh and Read, 1991). Stage 0 is the preparatory stage. In this stage, mother plants are grown ex vitro. In stage 1, an axenic culture of an explant is initiated. Stage 2 is the multiplication stage. Stage 3 is elongation and root induction or development stage. Stages 1 to 3 are in vitro stages. In stage 4, plants are transferred to greenhouses and acclimatized.

From the standpoints of utilization of the facility, the production of micropropagated plant involves two phases. The first phase consists of in vitro multiplication processes conducted under sterile conditions like a clean room (stages 1 to 3) and the second phase consists of ex vitro acclimation processes mainly done in a greenhouse (stage 4). The most costly part of the first phase is division and transplanting of plantlets in stage 2. However, Okamoto et al. (1998) developed a robotic system to automate the division and transplanting of stage 2 micropropagated sugarcane plantlets. A selective compliance assembly robot arm (SCARA) type manipulator and an end-effecter were used for dividing and transplanting the plantlets, and a machine vision system was used to detect the position and size of a clump of multiple shoots. A pilot plant was built on the Tokunoshima Island. Wang et al. (1999) developed another type of robotic system to automate the sub-culture of stage 2 micropropagated sugarcane. Specially-developed culture containers were used to facilitate shape recognition and division. The plantlets were grown between parallel plates which restricted the direction of their elongation.

Most of the processes of the second phase, such as watering, fertilizing, environmental control, soil preparation and moving of trays, have already been automated as the result of development in the field of cutting propagation and seedling production (Aitken-Christie, 1990). However, as with the production of any kind of micropropagated plant, multiple shoots must be divided and sorted, thus raising the production cost.

Micropropagated plantlets are grown thickly in culture vessels and their roots become entangled with each other, so the producer must separate them carefully into individual plantlets and transplant them into new trays or pots. In addition to separation, the plantlets must also be selected. Since the size of micropropagated plantlets is more irregular than that of plants which propagate by seeds, the supplier must sort them by their degree of growth to sell uniform transplants to farmers. These operations are currently done manually and account for the most of the cost of the acclimation process. However, Kaizu et al. (2001) developed and tested a prototype system for automating the division of micropropagated sugarcane shoots. Specially-designed end-effecters could divide 77% of shoots into individual shoots.

Figure 1 shows a view of the shoots separation system. Divided shoots are transplanted to the new tray according to their size. We are planning to use a flat belt conveyer to move the divided shoots from the separating robot system to a transplanting robot system. The transplanting robot system needs to identify the orientation, position and degree of growth of the shoots placed on the conveyer.

The objective of this research is to develop the algorithms for image processing, which recognize the 2-dimensional shape of individual shoots and estimate the degree of growth.

Many studies have been done on the shape recognition and sorting of agricultural products, particularly post-harvest fruits and vegetables. Some studies have also

investigated the shape recognition of plants which are still growing. Simonton et al. (1990) used image processing for shape recognition of geranium cuttings and succeeded in detecting the position of leaf blades, petioles and stems. Kaizu et al. (1996) approximated the boundary shape of an orchid seedling by using polar coordinates. Sixty-four equally spaced radial lines were drawn from the centroid and the length between the centroid and the boundary was measured in every angle. The series of lengths was then expanded into a Fourier series and the seedlings were sorted by size and patterns of Fourier coefficients which represented the shape of the seedlings.

Kondo et al. (1998) expressed the boundary of chrysanthemum cuttings by a chain code and estimated the orientation and position of the end of the petiole. Wang et al. (1998) developed a Hough transform-based algorithm to identify sugarcane shoots in a micropropagated stage 2 sugarcane shoot clump image.

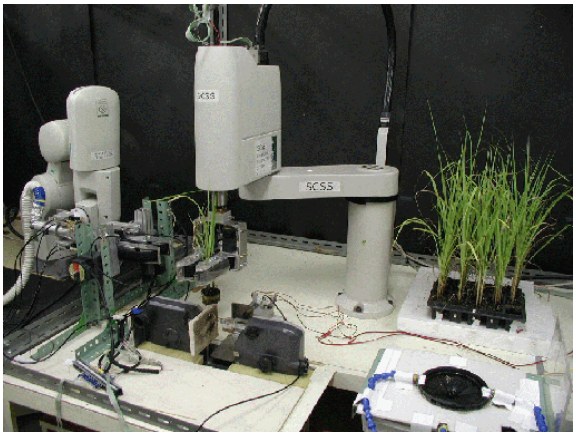

Figure 1. View of the shoot separation system

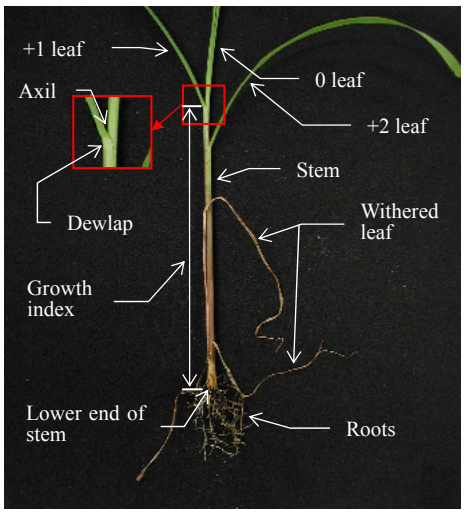

Figure 2. View of a micropropagated sugarcane shoot

Materials and methods

Micropropagated sugarcane shoot

Figure 2 shows a view of a divided micropropagated sugarcane shoot. The sugarcane cultivar used in this research was NiF 8. The leaves sprouted alternately. Each leaf was composed of a leaf blade and a leaf sheath. The joint part between a leaf blade and a leaf sheath is called a dewlap, but is also known as a blade joint or a joint triangle (Miyazato, 1986).

The dewlap acts as hinge between the leaf blade and leaf sheath. The highest fully developed leaf is called the +1 leaf and the second and third highest ones are the +2 leaf and +3 leaf and so on. Undeveloped leaves, which are higher than the +1 leaf, are called the 0, -1 and –2 leaves. Dewlaps can not be seen for these leaves.

As a standard way of measuring the degree of growth, we measure the distance between the lower end of the stem and the dewlap of the +1 leaf. However, this method may not be valid for measuring the true growth at the beginning and the end of the whole growth period. During the early days of growth, the length of a leaf sheath grows rapidly, so the sum of the true growth and the growth of a leaf sheath is the apparent growth. However, we must not break the shoots when sorting and transplanting them, so we must determine the growth only from visible indicators. This method should be practical for grouping,. In this research, we use the length between the highest dewlap

and the lower end of a main stem as an indicator of the growth.

Experimental apparatus

Figure 3 shows a view of the experimental apparatus. A digital camera (Olympus C3030) was used to acquire images of the shoots. The camera was mounted on a copy stand. A frame grabber (Hitachi IP-5000) and a personal computer (Intel Pentium II, 450 MHz) were used for image processing. This frame grabber has about 180 basic image processing routines, so a real-time application can be easily made (Hitachi, Ltd., 1998). A C++ compiler (Microsoft Visual C++ 6.0) was used to develop the application. We placed the shoots on a black velvet paper. As mentioned before, the shoots had alternate leaves, so they did not rotate on a stem axis. 500 W daylight bulbs with 5900 K color temperature were used for illumination. Shutter speed and aperture were set manually.

The digital camera was capable of taking an image at a resolution of 2048 x 1536. Two sizes of region were clipped from the original image for image processing as shown in Figure 4. The smaller region covered the stem root area and the larger one covered the whole plant area. Although, the shape could be recognized precisely from the higher resolution image, we reduced the resolution to 512 x 384 for real-time processing. We call the smaller image the "close image" and the larger image the "far image". The close image was used to find the lower end of the stem, which was the boundary between the stem and the root. The far image was used to detect the position of the dewlap. We plan to use two cameras to capture both images in future.

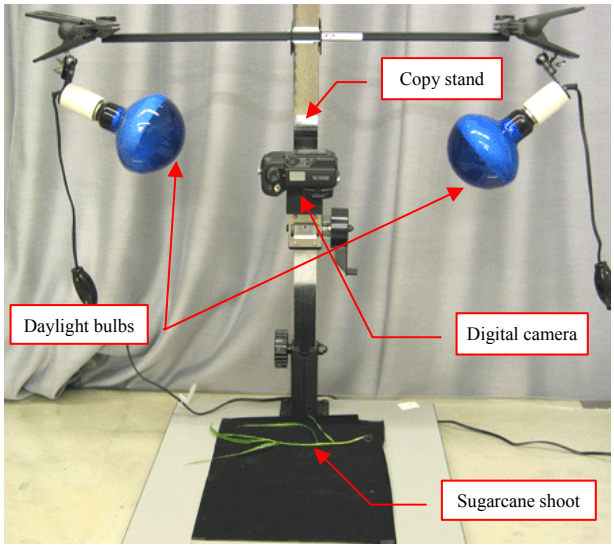

Figure 3. View of the experimental apparatus

Figure 4. Two types of image area: far image and near image

Calculation of the stem axis angle

The angle of the stem axis to the y-axis and its position in the image varies from image to image. A robot needs to know the angle and the position in order to pick out and transplant shoots. We used the Hough transformation (Duda and Hart, 1972) to calculate the stem axis angle and distance from the origin of the image to the stem axis. After detecting the stem axis, the image was rotated to make the main stem parallel to the y-axis, then shifted to move the main stem to the center of the image. This was done because misjudgment may occur in detecting the lower end of the stem if there is an

angle between the main stem and y-axis.

The boundary shape of the main stem was almost straight in each shoot (Figure 5(a)), and we used this characteristic to determine the stem direction. First, the shoot area was extracted from the original image by binarization (Hitachi, Ltd., 1998) (Figure 5(b)). Since the images were taken indoors under controlled lighting, the threshold value of binarization was set to be constant. After binarization, right edge points were located (Figure 5(c)). These points were then transformed into ρ–θ parameter space (Duda and Hart, 1972) and the line that passed through the largest number of edge points was determined. This line represented the right border of the stem. In the same manner, the left edge points shown in Figure 5(d) were located and then the most probable line was detected by Hough transformation. Figure 5(e) shows an image of two lines detected from the stem boundary. The stem axis was located at the center of those two lines. In Figure 5(f), the image was rotated and shifted, so the stem was parallel to the y-axis and was located at the center of the image.

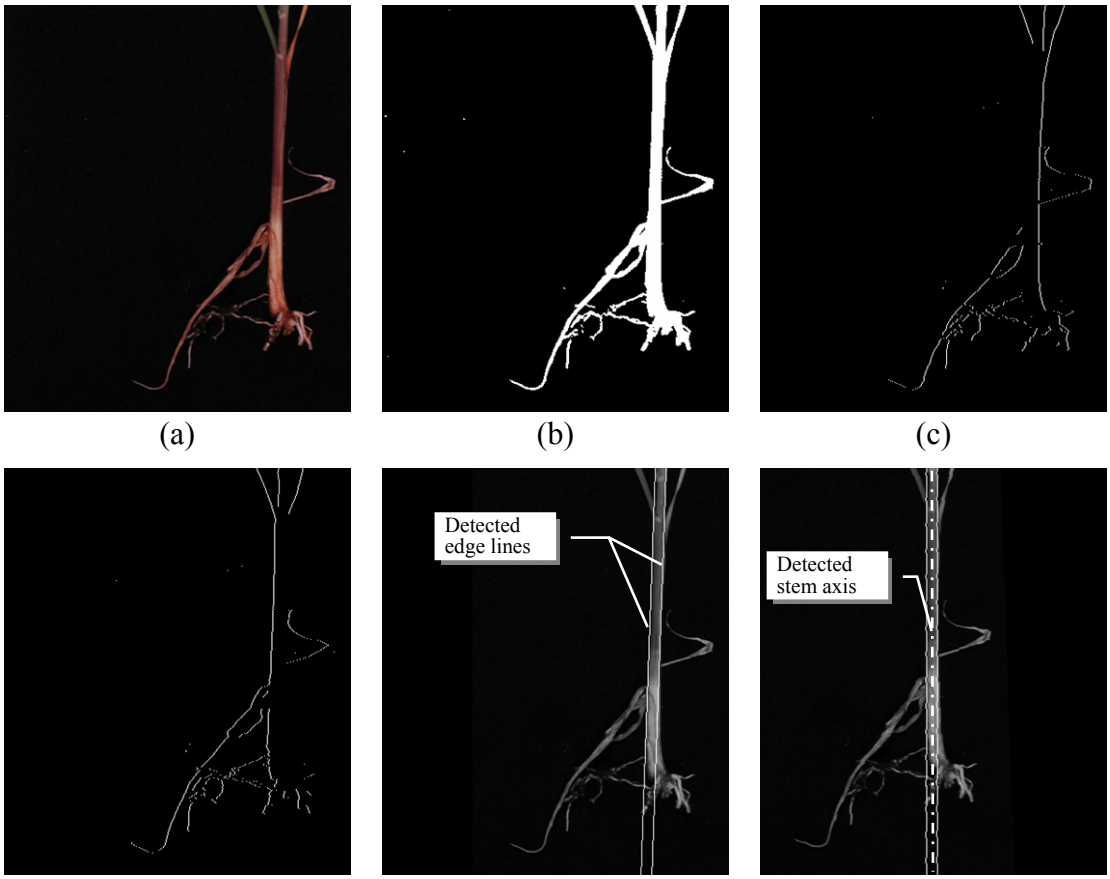

Figure 5. Calculating the stem angle and position (see text)

Detection of the lower end of the stem

The lower end of the stem is located between the stem and the roots. A human can distinguish the stem from the roots very easily. Our system recognized them as follows.

Stem: Straight, wide, continuous, parallel to y-axis and distributed around the center line of the stem

Roots: Crooked, narrow, discontinuous, grow radially and some of them are distributed away from the center line of the stem

These characteristics are relative indices in an individual shoot; the criteria must be changed adaptively for each shoots. We therefore designed a template as shown in Figure 6. The height of the template *Ht* was 20 pixels and the width *Wt* was two thirds of the width of the main stem *Ws*. The brightness of the left half of the template was 0 and that of the right half was 255. This template was designed not only for detecting the boundary shape but also for detecting the width of the object. The template was applied to the binary image and average residuals between the template and the binary image were calculated (Figure 7). The average residual $Ar(x,y)$ was expressed as:

$$Ar(x,y)=\frac{\sum_{n=0}^{Ht}\sum_{m=0}^{\frac{Wt}{2}-1} I(x+m-\frac{Wt}{2},y+n-Ht)+\sum_{n=0}^{Ht}\sum_{m=\frac{Wt}{2}}^{Wt}\left|I(x+m-\frac{Wt}{2},y+n-Ht)-255\right|}{HtWt} \quad (1)$$

where $I(p,q)$ was the brightness of the binary image at (p,q).

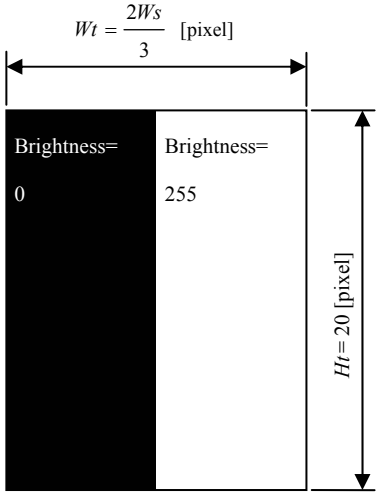

Figure 6. Template for detecting the main stem

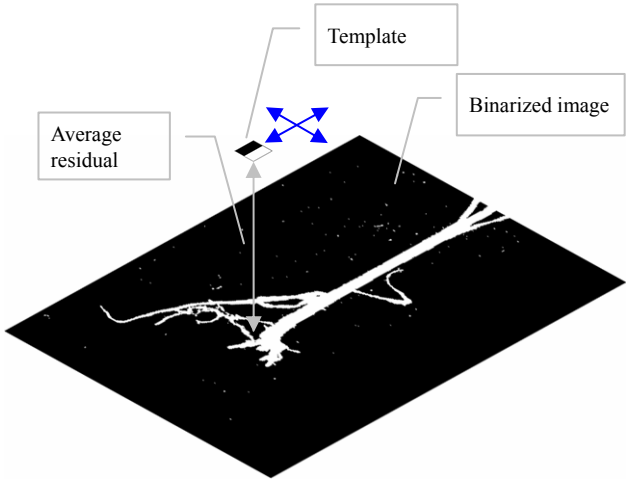

Figure 7. Applying the adaptive template to a binarized image

Figure 8(a) shows a binarized image of the shoot. Figure 8(b) shows an image in which the objects were eroded only vertically, then the largest region was extracted. The template was applied on this image. *Ws* was the width of the stem at the center of a region shown in Figure 8(b). The average residuals are shown in Figure 8(c). The average residuals at each coordinates were indicated by the brightness at these coordinates. In this image, the brightness was transformed into spectral color for ease of understanding.

The average residual indicates the straightness of the boundary shape. If the boundary is straight and parallel to the y-axis, the average residual becomes low where the boundary in the template and the boundary in the original image match. The average residual can also indicate the width of the object. The width of the template was set to be two thirds of the stem width, so if the right half of the template is fully overlapped with a wide object like the stem, the average residual becomes low, but if it is overlapped with a narrow object like the root, the average residual becomes high. The average residual was 128 where the brightness of the whole area in the original image

overlapped with the template is 0 or 255, and is very low at the left edge of the shoot and very high at the right edge of it.

Candidates for the stem boundaries had to satisfy the following inequalities:

$$Ar(x, y) < Kt / Wt \quad (2)$$
$$Ar(x, y) > 255 - Kt / Wt \quad (3)$$

where Kt is a constant set to 300. The threshold values are inversely proportional to the template width, because as the template width narrows, the average residual is more sensitive to the boundary shape. Figure 8(d) shows an example of an image of a stem boundary candidate region.

Some of the extracted regions may be roots or leaf blades (Figure 8(d)). To eliminate them, other criteria such as continuity (area), angle to the y-axis and horizontal distance from the stem centerline were calculated for each region. Figure 8(e) shows the final result of the detection superimposed on a gray image. Small regions were eliminated, so the stem boundaries were identified properly. The lowest point in the identified regions was defined as the y-coordinate of the lower end of the stem.

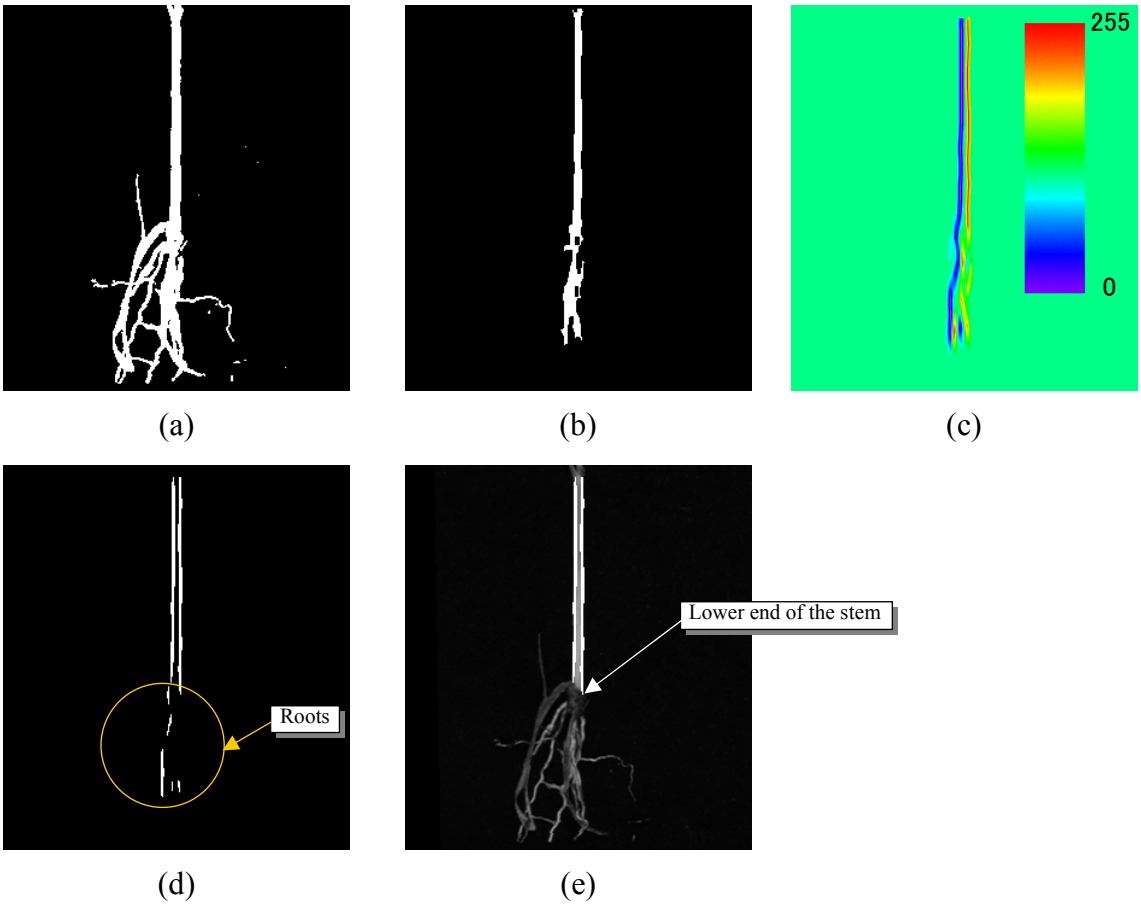

(a) (b) (c)

(d) (e)

Figure 8. Detection of lower end of the stem (see text)

Detection of the dewlap of +1 leaves

People can easily distinguish the position of the dewlaps in an image because our eyes are able to recognize the boundary shape features of the shoots. The distinctive boundary shape features of a sugarcane shoot are as follows.

- Stem: straight
- Leaf blade: curves gently
- Tip of leaf blade: acute angle
- Axil: inversely acute angle
- Dewlap: obtuse angle at the joint of a leaf blade and a leaf sheath
- Root: irregular, repeats big changes in a short period

Besides boundary shape, the colors of shoots are also important features. Each part of a sugarcane shoot has the following colors.

- Stem: red, green and white
- Leaf blade: green
- Root: brown and white
- Dewlap: white

In this research, the following algorithms utilizing the shape and color features were developed to find the highest dewlap position.

Extraction of a dewlap search region

Almost all the shoots had brown withered leaves. They were often bent irregularly, so that they crossed over a stem or a viable leaf blade. Since the +1 leaf's dewlap was detected on the assumption that leaf blades would come out alternately, we could not trace the right boundary if withered leaves existed in an image. So, we eliminated them before the dewlap detection.

First, a YIQ image was transformed into an HSI image (Hitachi, Ltd., 1998). Fig 9(a) shows a hue image. In this image, the bright region was presumed to be green. We identified this region (Figure 9(b)). The green region consists of viable leaves and parts of the stem. In addition, the Y image was binarized, then it was eroded three times only along the y-axis to eliminate the withered leaves. To restore the shape of the uncut region, the image was dilated the same number of times and the largest region was selected (Figure 9(c)). Although some viable leaf blades were eliminated in this process, by logically adding the image shown in Figure 9(b), withered leaves could be eliminated (Figure 9(d)). The extracted area was considered as the dewlap search region.

Boundary tracking

Clockwise boundary tracking was performed on the dewlap search area. The y-coordinate of the start point was the same as the y-coordinate of the lower end of the stem. Numbers from the start n, called boundary numbers, and coordinates $(Xp(n), Yp(n))$ were recorded.

Chain coding expressing the moving direction of adjacent pixels on a boundary is one way to provide for shape recognition. Kondo et al. (1998) succeeded in detecting petioles of chrysanthemum cuttings by the frequency of the chain codes. Since the chain code expresses the moving direction of neighboring pixels, curvatures of the boundary pixels are limited to -180, -135, -90, -45, 0, 45, 90 and 135 degrees (Figure 10).

We calculated a boundary curvature which was defined by an exterior angle formed with the present boundary pixel and pixels 20 pixels apart from it in the backward and forward directions to increase the angular resolution and noise-robustness. The boundary curvature $\theta p(n)$ was calculated and recorded for all the boundary pixels. Figure 11 shows the curvatures at a dewlap, the tip of a leaf and an axil.

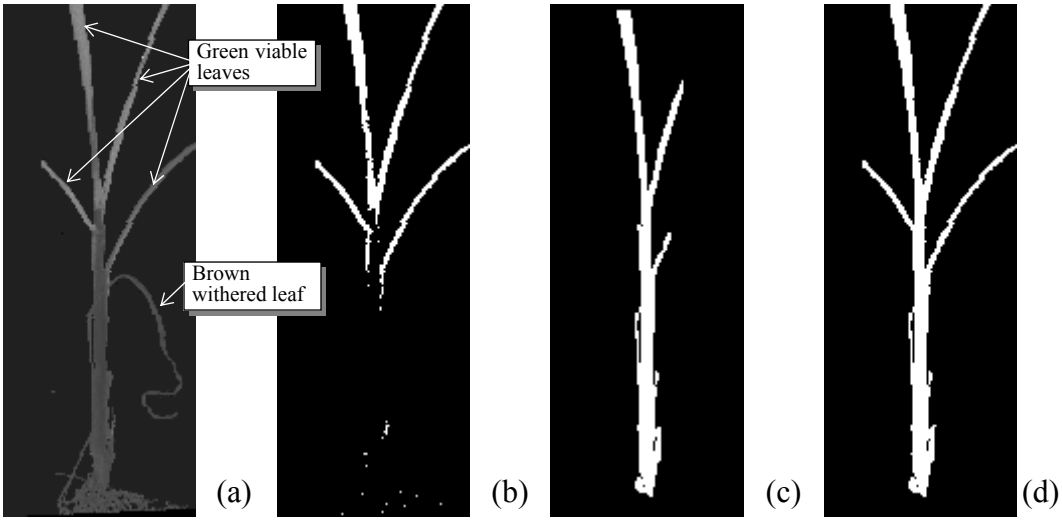

Figure 9. Dewlap search area extraction (see text)

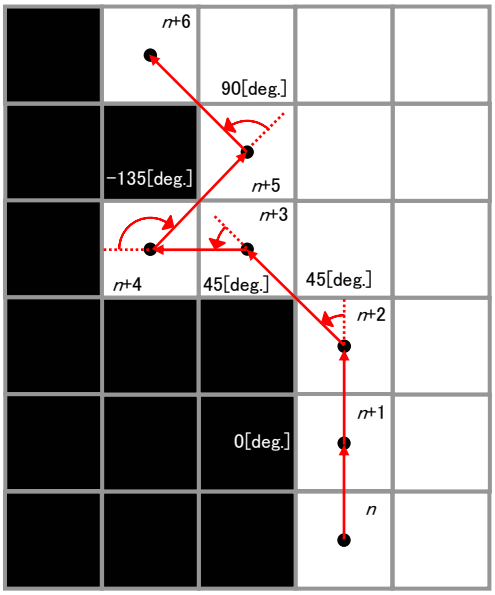

Figure 10. Boundary tracking

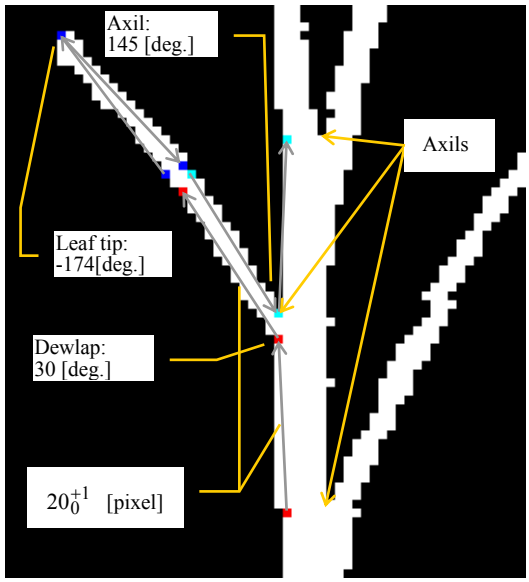

Figure 11. Boundary curvatures at a dewlap, a leaf tip and an axil

The +1 leaf dewlap detection

The leaf tips, or axils were clearly detected from the boundary curvature. On the other hand, the dewlaps located on the outside of the axils could not be detected directly, because the curvature at the dewlap was not clearly distinguishable in that neighborhood. Therefore the axils that corresponded to the dewlaps were detected first, and then the dewlaps were determined based on the locations of the axils. The boundary pixels that satisfied the following inequalities were determined as candidates for axils:

$$\theta p(n) \geq 115[\text{deg.}] \quad (4)$$

$$Xc - Ws < Xp(n) < Xc + Ws \quad (5)$$

where θp is the function of the boundary curvature, n is the boundary number, Xc is the x-coordinate of the stem axis, Ws is the width of the stem, and Xp is the function of the x-coordinate of the boundary.

If two or more pixels satisfied these inequalities at one axil, the nearest one to the low end of the stem was selected as the true axis. The detected axils were sorted by the distance from the low end of the stem. The pair (Xa_i,Ya_i) consists of the x and y coordinates of the ith highest axil.

The objective of this process was to detect the dewlap of the +1 leaf. However the structure of each shoot differed according to its degree of growth and facing direction, so the shoots were divided into the following seven cases.

Case 1: The number of axils was 0. In other words, the shoot had only one leaf and it was very small. Such shoots were set aside and would not be transplanted

Case 2: There was one axil. Seen from the axis, the slope of left leaf was gentler than that of the right leaf as follows:

$$\left|Xb(n) - Xa_1\right| \geq \left|Xa_1 - Xf(n)\right| \quad (6)$$

where $Xb(n)$ and $Xf(n)$ are x-coordinates of pixels which are 20 pixels from the present pixel, and Xa_1 is the x-coordinate of the highest axil.

Figure 12(a) shows the structure of the plant. In this case, the leaf at the left side of the axil was thought to be the +1 leaf, so the left side of the shoot was searched as shown in Figure 12(a). In the dewlap search section, the following angle was calculated:

$$\theta d(o) = \theta p(o) - \theta s(o) \quad (7)$$

where $\theta s(o)$ is the angle between the boundary vector and the stem shown in Figure 13(a). The maximum $\theta d(o)$ indicated the position of the +1 dewlap.

As stated previously, a dewlap is the joint of a leaf blade and a leaf sheath i.e. a stem. It is detected reliably by taking the angle between the y-axis and the boundary vector $\theta s(o)$ from the boundary curvature $\theta p(o)$. If we determined the pixel that maximized only $\theta p(o)$ as the dewlap, the false pixel would be identified, but the pixel that maximized $\theta d(o)$ would locate the true dewlap on the boundary (Figure 14).

Case 3: Although there was one axil, if the inequality (6) was not satisfied, the right side of the shoot was searched (Figure 12(b)). $\theta s(o)$ is the angle shown in Figure 13(b).

Case 4: There were 2 or more axils. The boundary number of the highest axil p and that of the second highest one q were compared. If p was smaller than q, the left side of the shoot was searched (Figure 15(a)).

Case 5: There were 2 or more axils, but the order of the boundary number of the highest and second highest axil was different from case 4, so the right side of the shoot was searched (Figure 15(b)). $\theta s(o)$ is the angle shown in Figure 13(b).

Case 6: The order of axil height was the same as in case 4, but if any of the following conditions were satisfied, the dewlap corresponding to the second highest axil was determined as the +1 leaf's dewlap.

(a) $Wl > 2Wr$ (8)

where Wl and Wr are leaf width at the left and right sides of the highest axil, respectively (Figure 16(a)). We based this on the fact that a -1 leaf was generally narrower than a 0 leaf.

(b) $\theta d(o) < 8.5$ [deg] (9)

where $\theta d(o)$ is the maximum angle detected in case 4. If there was no dewlap in the search section, $\theta d(o)$ became less than 8.5 degrees.

(c) $Red(Xp(n),Yp(n)) < 0.95Green(Xp(n),Yp(n)) \quad (n \in S)$ (10)

$Red(Xp(n),Yp(n)) < 100 \quad (n \in S)$ (11)

Red and *Green* are the red and green brightness of boundary pixels. *Xp* and *Yp* are the x and y-coordinates of the boundary. *S* is the set of boundary numbers included in the dewlap search section. As mentioned previously, the dewlaps were white. If there was no dewlap in the search section, the inequalities (10) and (11) were satisfied. The leaf blade was green, so the red brightness in the search section was lower than the green brightness.

Case 7: There were 2 or more axils and the order of the axil height was the same as in case 5, but if the following inequalities were satisfied, the dewlap corresponding to the second highest axil was determined as the +1 leaf's dewlap. The dewlap search section is shown in Figure 16(b).

$2Wl < Wr$ (12)

$\theta d(o) < 8.5$ [deg] (13)

$Red(Xp(n),Yp(n)) < 0.95Green(Xp(n),Yp(n)) \quad (n \in S)$ (14)

$Red(Xp(n),Yp(n)) < 100 \quad (n \in S)$ (15)

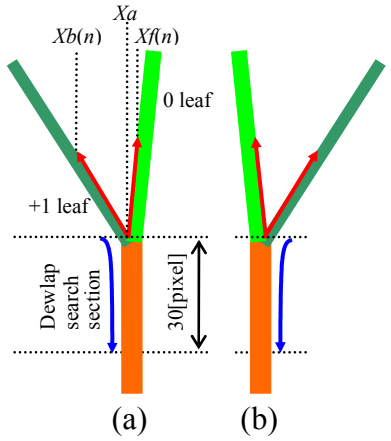

Figure 12. Results for one axil
(a) case 2, (b) case 3

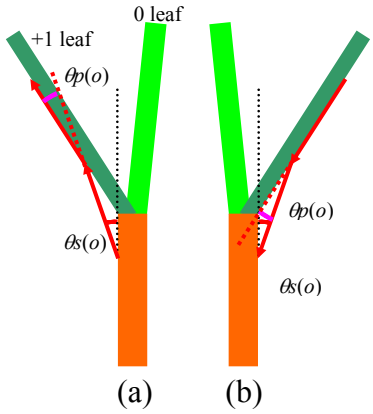

Figure 13. Boundary angles for determining +1 leaf dewlap position

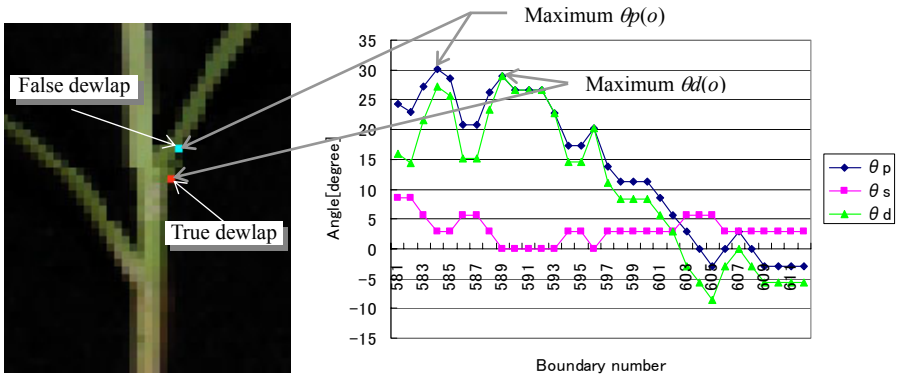

Figure 14. Locating the dewlap by taking $\theta s(o)$ from $\theta p(o)$

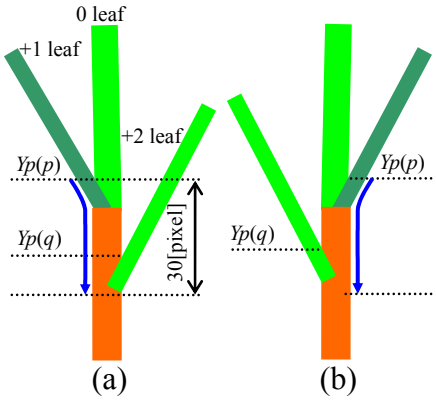

Figure 15. Results for 2 or more axils.
(a) case 4, (b) case 5

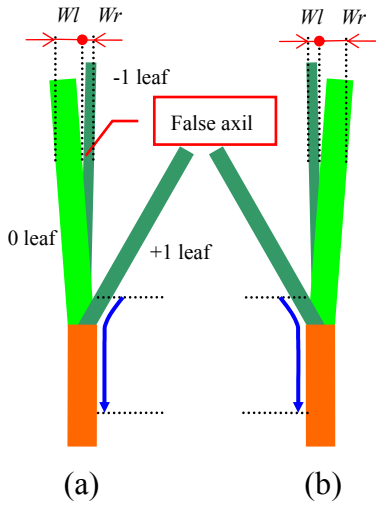

Figure 16. (a) case 6, (b) case 7

Results and discussion

Images of 52 shoots were taken. In the close image, 1 pixel was equivalent to 0.148 mm, and in the far image, 1 pixel was equivalent to 0.297 mm. The results were as follows.

Detection of the stem angle

Table 1 shows the results of stem angle calculations using edge detection of a binarized image and Hough transformation. The stem angles were measured by hand using Adobe Photoshop 7.0, then were compared with the calculations. The stem angle of most shoots was detected properly (Figure 5(f)).

The stem axis angle detection is based on the assumption that the stem is straight, therefore the maximum error occurred when the stem was bent at the middle (Figure 17). The detection algorithm chose the most likely line, so the center line of the upper half of the stem was detected.

Table 1. Results of the stem angle calculation. SE: Standard error

SE [degree]	1.5
Maximum error [degree]	8.3

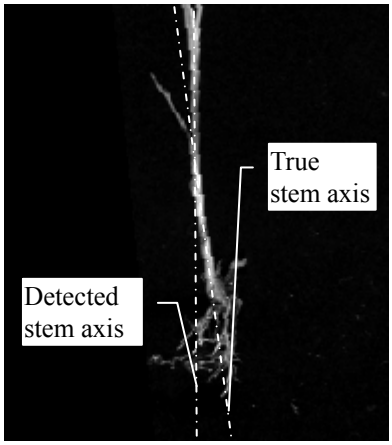

Figure 17. Error in stem angle detection

Detection of the lower end of the stem

Table 2 shows the results of detecting the lower end of the stem. In the image, which had already been rotated and shifted, the coordinates of the lower end of the stem were located by hand using the same method as the angle detection. Then the true coordinates were compared with the coordinates located by the algorithm. By changing the width of the template proportionally to the stem width, the lower end of most of the shoots was properly detected as shown in Figure 8(e). Considering that the stem width ranged from 1 to 3 mm, the standard error of the distance was acceptable.

Table 2. Results of detecting the lower end of the stem

	X-coordinate [mm]	Y-coordinate [mm]	Distance [mm]
SE	0.6	1.9	2.0
Maximum error	2.4	6.8	6.8

The error in the x-coordinate resulted from the error in the stem axis angle detection. Actually, the shoot giving rise to the maximum error in the x-coordinate detection was the same as that which had the maximum error in the angle detection. The maximum error in the y-coordinate resulted from the fact that the vertically grown shoots were overlapped; as a result, they were recognized as stems and could not be eliminated.

The +1 leaf dewlap detection

Table 3 shows the number of shoots belonging to each case. It also shows the success rate of side detection, which detects on which side the dewlap is. This table shows the degree to which the algorithm could recognize the shoot structure properly. The shoot in case 1 was removed, so it was not added to the total. The structures of the shoots in the cases 2, 4 and 6 were same as these of the shoots in the case 3, 5 and 7, so they were added respectively.

There three causes of the errors. 1) a withered leaf was not properly eliminated, because it was parallel to a stem, 2) width of the +1 leaf was too narrow, so the +1 leaf was cut off during the eroding process, and 3) a 0 leaf was almost fully developed, so it was regarded as a +1 leaf.

Table 3. Success rate of +1 leaf dewlap side detection

	Number	Succeeded	Failed	Success rate
Case 1	(1)	-	-	-
Case 2, 3	12	11	1	91.6%
Case 4, 5	28	26	2	92.9%
Case 6, 7	11	8	3	72.7%
Total	51	45	6	88.2%

Table 4. Results of detecting the +1 leaf dewlap

	X-coordinate [mm]	Y-coordinate [mm]	Distance [mm]
SE	0.6	2.3	2.4
Maximum error	2.7	12.5	12.5

Table 4 shows the difference between the dewlap detected by the algorithm and those identified by sight. For the properly recognized shoots, the error was lower than the standard error. On the other hand, if the shape recognition failed, the error became large. To improve the accuracy of the dewlap detection, the withered leaves should be taken off physically prior to the shape recognition.

Figure 18 (a) shows the results of the shoot in case 4 and (b) shows the shoot in case 6. The left ends of the short bars indicate the axils and the right end in Figure 18 (a) and the left end in Figure 18 (b) of the middle length bar indicate the +1 leaf's dewlaps. The long bars crossing the stem indicate the lower end of the stem. The relative positions of the highest axil and the second highest axil are the same in these two images though the dewlaps were detected on different sides of the shoots.

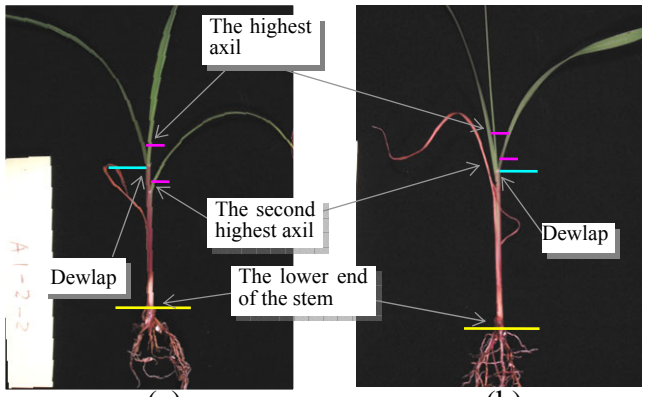

Figure 18. Results of the dewlap detection. (a) case 4, (b) case 6

Measurement of the growth index

The growth index was the difference between the y-coordinate of the dewlap and the lower end of the stem. Table 5 shows principal statistics of the growth index measured by hand. The growth index of the maximum shoot was seven times as large as that of the minimum shoot.

Table 6 shows the results of calculating the growth index by the algorithms. The standard error was 2.7 mm and the standard error of error ratio was 6.4%. The relation between the growth index measured by hand and that by the program is shown in Figure 19. In a future work, we will measure the length of the shoots sorted by a human operator and verify the validity of the algorithm we developed.

Table 5. Principal statistics of the growth index

	[mm]
Minimum value	18.4
Maximum value	135.8
Mean value	60.0
SD	27.6

Table 6. Calculated the growth index

	[mm]	[%]
SE	2.7	6.4
Maximum error	6.8	22.6

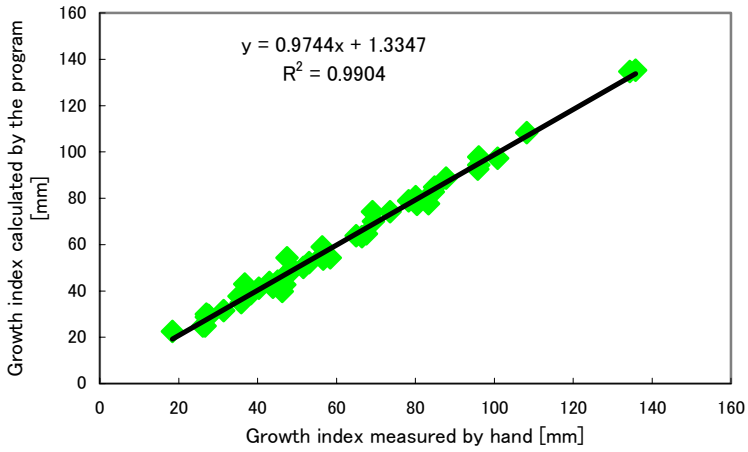

Figure 19. Growth index measured manually and calculated by the program

Conclusions

Machine vision algorithms were developed for shape recognition and growth measurement of ex vitro micropropagated sugarcane shoots. Shape features, such as stem axis angle, position and degree of growth required for robotic sorting and transplanting systems were measured by a newly developed program. The following results were obtained.

(a) The Hough transformation was capable of detecting the straight lines of both sides of the main stem. From these two lines, the position and the angle of the stem axis could be estimated.

(b) By calculating average residuals between a newly developed half-black, half-white template and a binarized image of a shoot, the boundary region of the stem could be identified. The width of the template was proportional to the width of the stem, so the lower end of the stem could be detected accurately irrespective of the size of the shoots.

(c) The curvature of boundary expressed well the characteristic of the boundary shape. From the boundary curvature, we could find the axils, the leaf tips and the dewlaps. The red and green brightness also helped us to estimate the dewlap. However it was difficult to determine the dewlap of the +1 leaf, if the 0 leaf was almost fully developed.

(d) In future work, we would like to verify the validity of the algorithm by applying these results to real robotic picking and sorting operations.

Acknowledgements

We would like to thank Mr. Yuei Taba and Nansei Togyo Co., Ltd. for supplying the micropropagated sugarcane and giving us valuable advice and suggestions. We also acknowledge graduate student Mr. Ryota Hayashi for helping with the programming. This research was financially supported by a Grant-in-Aid for Scientific Research from the Ministry of Education, Culture, Sports, Science and Technology of Japan (Project No. 11556044).

References

Aitken-Christie, J. 1991. Automation. In *Micropropagation Technology and Application*. ed. P. C. Deberg and R. H. Zimmerman, 363-388. Dordrecht, The Netherlands: Kluwer Academic Publishers.

Debergh, P. C. and P. E. Read. 1991. Micropropagation. In *Micropropagation Technology and Application*. ed. P. C. Deberg and R. H. Zimmerman, 1-13. Dordrecht, The Netherlands: Kluwer Academic Publishers.

Duda, R. O. and P. E. Hart. 1972. Use of the Hough transform to detect lines and curves in pictures. *Communications of the ACM* 15(1): 11-15.

FAOSTAT Agriculture Data. 2002. Sugarcane production in 2001. *http://apps.fao.org*. Accessed 11 July 2002.

IP-5000/CD Programming Manual. 1998. : Hitachi, Ltd.

Kaizu, Y., T. Okamoto, O. Kitani and T. Torii. 1996. Classification of cultivated seedling of orchid using machine vision. *Journal of the Japanese Society of Agricultural Machinery* 58(2): 49-56.

Kaizu, Y., T. Okamoto and K. Imou. 2001. System for Automatic Separation of *Ex Vitro* Micropropagated Sugarcane. *Agricultural Engineering International: the CIGR Journal of Scientific Research and Development* Vol. III, December: 1-17.

Kondo, N., Y. Ogawa and M. Monta. 1998. Basic studies on automatization of chrysanthemum cutting sticking operation (Part 1) –Development of chrysanthemum cutting recognizing algorithm by use of color image and chain code-. *Journal of the Japanese Society of Agricultural Machinery* 60(2): 67-74.

Miyazato, K. 1986. *Sugarcane and its cultivation*, 60-61. Naha, Japan: Nihon Bunmitsuto Kogyokai.

Okamoto, T., C. S. Zhao, Y. Miyama, T. Torii and K. Imou. 1998. Robotic sugar cane seedling propagation system in tissue culture. *Journal of the Japanese Society of Agricultural Machinery* 60(6): 71-77.

Redenbaugh, 1991. Applications of micropropagation for agronomic crops. In *Micropropagation Technology and Application*, ed. P. C. Deberg and R. H. Zimmerman, 285-310. Dordrecht, The Netherlands: Kluwer Academic Publishers.

Simonton, W. and J. Pease. 1990. Automatic plant feature identification on geranium cuttings using machine vision. *Transactions of the ASAE* 33(6): 2067-2073.

Taba, Y., Y. Miyama, K. Ikeda, N. Kamezawa and K. Sawada. 1998. Production of sugarcane mericlone plants. *Proceedings of the Research Society of Japan Sugar Refineries Technologists* 46: 29-34.

Teruya, H. and M. Tokumoto. 1999. Clonal propagation of sugarcane meristem culture (3) Characteristics of growth and ability of tissue cultured seedling. *Japanese Society of Tropical Agriculture* Vol. 43 Extra issue 2:15-16.

Wang, Z., P. H. Heinemann, H. J. Sommwe III, P. N. Walker, C. T. Morrow and C. Heuser. 1998. Identification and separation of micropropagated sugarcane shoots based on the Hough transform. *Transactions of the ASAE* 41(5): 1535-1541.

Wang, Z., P. H. Heinemann, P. N. Walker and C. Heuser. 1999. Automated micropropagated sugarcane shoot separation by machine vision. *Transactions of the ASAE* 42(1): 247-254.

Kaizu, Y., T. Okamoto, and K. Imou. “Shape recognition and Growth Measurement of Micropropagated Sugarcane”. Agricultural Engineering International: the CIGR Journal of Scientific Research and Development. Manuscript IT 02 003. Vol. IV. October 2002.